ISOTOPE EFFECTS ON THE FUNDAMENTAL BAND GAP OF LEAD SULFIDE

by

Haijun Lian

B.S., Beijing Normal University, China, 2002

A THESIS SUBMITTED IN PARTIAL FULFILLMENT
OF THE REQUIREMENTS FOR THE DEGREE OF

MASTER OF SCIENCE

In the Department
of
Physics

SIMON FRASER UNIVERSITY
Fall 2005

APPROVAL

Name: Haijun Lian

Degree: Master of Science

Title of thesis: Isotope Effects on the Fundamental Band Gap of Lead Sulfide

Examining Committee: Dr. Howard Trottier, Professor, Department of Physics
Chair

Dr. Mike Thewalt, Professor
Senior Supervisor, Department of Physics

Dr. Karen Kavanagh, Professor
Supervisor, Department of Physics

Dr. George Kirczenow, Professor
Supervisor, Department of Physics

Dr. Simon Watkins, Professor
Examiner, Department of Physics

Date Approved: August 26, 2005

SIMON FRASER UNIVERSITY

Partial Copyright Licence

Abstract

Lead sulfide (PbS) is one of the oldest known semiconductors, occurring naturally as the mineral galena. One of its interesting properties is a strong increase of the band gap energy with increasing temperature, opposite in sign to almost all other semiconductors. We report on the isotope shift of the band gap energy between natural PbS (containing mostly ^{32}S) and PbS made with enriched ^{34}S, measured using low temperature photoluminescence spectroscopy. The observed isotope shift is also opposite to the normal expectation of larger band gap for the heavier mass. In addition, we report on improved measurements of the temperature dependence of the band gap energy measured using absorption spectroscopy, to study the expected connection between the isotope shift of the band gap energy and its shift with temperature.

To my friends around the world.

“夫君子之行：静以修身，俭以养德。非淡泊无以明志，非宁静无以致远。”

—诸葛亮《戒子篇》

Acknowledgments

First of all, I would like to express my gratitude and respect for my senior supervisor, Dr. Mike Thewalt. Without his invaluable guidance and continuous support, the project would not have been possible.

I am grateful to all the members of the Thewalt lab, past and present. Special thanks to Michael Steger, for his many hours of proofreading and software support, and Albion Yang, for helpful discussions concerning the experimental aspects of the project.

I also thank our collaborator Manuel Cardona for providing us with the isotopically enriched lead sulfide samples and for his contribution to the scientific work.

I am indebted to all Chinese fellows in the Department of Physics at Simon Fraser University, in particular to Zhiyi Liu, who introduced me into the magic LaTeX world, and Weiyang Jiang, who provided invaluable academic advice.

For their generous financial support, I would like to acknowledge Simon Fraser University, Department of Physics and Dr. Mike Thewalt.

Finally, thanks to my parents and my brother for their moral support.

Contents

List of Tables

List of Figures

Chapter 1

Introduction

Only in the past few years has it been affordable to produce highly isotopically enriched, chemically pure and near perfect semiconductor crystals. This has led to a renaissance in the study of isotope effects (the effects of isotopic composition) in semiconductors and produced one of the most important and active fields in condensed matter [1] [2]. The comprehensive research on isotope effects in semiconductors recently has been well summarized into three categories: phonon effects related to average isotopic masses, phonon effects related to isotopic disorder and effects of the electron-phonon interaction on the fundamental optical spectra [1].

One of the most important properties of semiconductors is the electronic band gap (we confine ourselves to the fundamental band gap in this thesis), which certainly is of the greatest importance for both fundamental research and industrial applications. Isotope effects on the band gap of the electronic band structure are macroscopically shown as the isotope shift of the band gap (change of the band gap as a function of isotopic composition) and the zero-point renormalization of the band gap (change of the band gap at zero temperature due to the zero-point vibration) [3]. Electron-phonon interaction and volume changes are the underlying microscopic mechanisms. The investigations have been conducted on most available isotopic materials (table III in [1]) and we continue the systemic research on the isotope effects in lead sulfide.

Lead sulfide (PbS) which occurs naturally as the mineral Galena, is one of the earliest known semiconductors, used originally in crystal radios, and still used today in inexpensive infrared detectors [4] [5]. PbS, similar to PbSe and PbTe in the family of lead chalcogenides, crystallizes in the sodium chloride (rocksalt) structure. It consists of equal numbers of lead

and sulfur ions placed at alternate points of a simple cubic lattice, in such a way that each ion has six of the other kind of ions as its nearest neighbors [6]. The structure can be described as a face-centered cubic Bravais lattice with a basis consisting of a lead ion at the origin and a sulfur ion at the center of the conventional cubic cell $(a/2)(\hat{x}+\hat{y}+\hat{z})$, where a is the side length of the cube or lattice constant. PbS is a direct-band-gap semiconductor with extrema of both conduction and valence bands occurring at the $L = (\pi/a)(1,1,1)$ point on the Brillouin zone face. The narrow band gap is 289.4 meV at 4.2 K and 418.9 meV at 300 K, which falls into the mid-infrared region. Also PbS possesses an abnormal positive temperature coefficient of the band gap: its band gap strongly increases with increasing temperature.

In this thesis, we have directly observed and measured the isotope shift of the band gap in lead sulfide due to the changes of sulfur isotopic masses at low temperature. In order to obtain the zero-point renormalization of the band gap, we have made the measurements of the temperature-dependent band gap for natural PbS in the range of 1.6 K to 320 K. Our measurements show much improvement compared to the ones reviewed in 1983 (page 35 in [7]). We then apply two simplified models to understand the temperature dependence of the band gap due to both the thermal expansion and the net electron-phonon interaction.

Chapter 2

Theoretical Framework

In this chapter, the theories applied in Chapter 4 are introduced. The following topics are discussed: how to determine the band gap of direct-transition semiconducting materials using absorption spectroscopy, how to determine isotope shifts of the band gap using low temperature photoluminescence spectra and how to determine the zero-point renormalization of the band gap using its temperature dependence.

2.1 Absorption of Light in Semiconductors

When a semiconductor is illuminated by a beam of light, photons interact with intrinsic electrons, localized electrons of defects and lattice vibrations at the surface and inside the medium [8]. Among various optical processes induced by electromagnetic waves, reflection and absorption are the strongest parts because those involve the lowest-order interaction of photons and fundamental excitations of the medium. Absorption is defined as the process in which incident radiation energy is retained without reflection or transmission on passing through a medium. The capability of absorption can be physically characterized by an absorption coefficient $\alpha(\omega)$. As a function of the energy of incident photons $\hbar\omega$, $\alpha(\omega)$ can provide the information of electronic band structures of semiconductors. Other macroscopic optical constants, such as the extinction index (the imaginary part of the complex refractive index) and the imaginary part of the complex dielectric function, can also be directly deduced from $\alpha(\omega)$. Furthermore, the refractive index and the real part of the complex dielectric function can be indirectly calculated by the Kramers-Kronig relations.

2.1.1 Quantum-Mechanical Description of Optical Absorption

When light travelling along the z axis is absorbed upon passing through a medium, the intensity of light decreases exponentially, with Beer-Lamberts law [8] [9]:

$$I(z) = I_0 e^{-\alpha z} \tag{2.1}$$

where α is the absorption coefficient of the material, the physical quantity that describes how strongly the medium interacts with electromagnetic waves in form of absorption processes. The optical penetration length α^{-1}, is the characteristic length that light travels in the medium when the intensity of light decreases by a factor of e.

The absorption coefficient could also be defined as the ratio between the rates at which energy is absorbed per volume V and the incident energy per unit area:

$$\alpha(\omega) = \frac{\hbar\omega P_{fi}}{I(\omega)V} \tag{2.2}$$

Here $\hbar\omega$, $I(\omega)$ and P_{fi} are respectively the energy of incident photons, the intensity of incident light and the quantum-mechanical probability for the transition rate of a system changing from the initial state $|i\rangle$ to the final state $|f\rangle$.

The electron-radiation interaction hamiltonian H' under weak external fields, which are the origin of the absorption process, can be expressed as:

$$H' = -\frac{e}{m} pA \tag{2.3}$$

where e, m, p and A are the electronic charge, mass, momentum of electrons and a vector potential, respectively. The semi-classical model of electron-radiation interaction is applied and only linear optical properties are considered in (2.3). Hence, following the formulism of [9], the transition probability P_{fi} in (2.2) can be obtained under the first-order approximation of perturbation theory in terms of $H'_{fi}(0)$, the matrix element of H':

$$P_{fi} = \frac{2\pi \left| H'_{fi}(0) \right|^2}{\hbar^2} \delta(\omega_{fi} - \omega) \tag{2.4}$$

(2.4) is one specific case of Fermi's golden rule. The matrix element $H'_{fi}(0)$ can be evaluated by the time-dependent perturbation theory shown in the following:

$$\left| H'_{fi}(0) \right|^2 = \frac{e^2 I(\omega) \left| p_{fi} \right|^2}{m^2 \epsilon_0 c \omega^2 n} \tag{2.5}$$

where c, ϵ_0, n and p_{fi} are the speed of light in vacuum, the dielectric constant in vacuum, the refractive index (the real part of the complex refractive index) and the momentum matrix element, respectively. When we bring Formula (2.3), (2.4) and (2.5) back into (2.2), we finally obtain the general expression for the absorption coefficient:

$$\boxed{\alpha(\omega) = \frac{2\pi}{V}\frac{e^2\left|p_{fi}\right|^2}{m^2\epsilon_0 cn\omega}\delta(\hbar\omega_{fi} - \hbar\omega)} \tag{2.6}$$

(2.6) is the general formula of discussion in various cases of absorption. The following subsection discusses the application in the case of direct and allowed transitions. Here an allowed transition corresponds to a finite dipole matrix element at the position of the minimum energy difference between valence and conduction bands. A direct transition means that the transition takes place at the same point of valence and conduction bands in the reciprocal space.

2.1.2 Direct and Allowed Transitions in the Absorption Edge

The joint density of states $\sigma_{CV}(\omega)$ between the conduction and valence bands is introduced when we evaluate the matrix element p_{fi} in (2.6) [8]. It is defined as the density of states available for a given transition energy $\hbar\omega$. If the bands are isotropic and parabolic in the region near the band gap, the valence band energy ϵ_V and conduction band energy ϵ_C near the band gap can be expressed as:

$$\epsilon_V = \frac{\hbar^2 k^2}{2m_V^*} \qquad\qquad \epsilon_C = \frac{\hbar^2 k^2}{2m_C^*} + E_g \tag{2.7}$$

where m_V^* and m_C^* are the effective masses of holes in the valence band and electrons in the conduction band. k is the particle wave vector as measured from the wave vector at the band edge. σ_{CV} correspondingly has the form of:

$$\sigma_{CV}(\omega) = \begin{cases} V\frac{(2\mu^*)^{3/2}}{2\pi^2\hbar^3}\sqrt{\hbar\omega - E_g} & \text{for} \quad \hbar\omega > E_g \\ 0 & \text{for} \quad \hbar\omega < E_g \end{cases} \tag{2.8}$$

where μ^* is the reduced effective mass of electrons and holes.

With the help of the joint density of states, we finally reach the expression which is convenient and important for experimental purposes:

$$\boxed{\alpha(\omega) = \begin{cases} B\sqrt{\hbar\omega - E_g} & \text{for} \quad \hbar\omega > E_g \\ 0 & \text{for} \quad \hbar\omega < E_g \end{cases}} \tag{2.9}$$

where B is a constant given by:

$$B = \frac{e^2(2\mu^*)^{3/2}}{12\pi^5 m^2 n \epsilon_0^2 c\hbar^3} |p_{CV}|^2 \tag{2.10}$$

So the transition for electrons from the valence band to the conduction band starts with an energy equal to E_g. When the energy of photons increases from below the band gap to above the band gap, the corresponding absorption coefficients increase abruptly from ~ 0 to $10^4 \sim 10^6$ cm^{-1} for most materials. The abrupt rising part of the absorption spectrum is called the absorption edge. From (2.9), the absorption coefficient is proportional to $(\hbar\omega - E_g)^{1/2}$ above the band gap. We can fit the squared absorption coefficient to a straight line and the corresponding intercept with the horizontal line of zero absorption coefficient gives the band gap energy E_g.

2.2 Photoluminescence in Semiconductors

2.2.1 Concepts

Whereas above band gap absorption in semiconductors is a process in which electrons are excited from the valence band to the conduction band by photons, luminescence is the inverse: electrons in the conduction band and holes in the valence band recombine and emit radiation [8] [10]. Luminescence processes can be divided into three distinct steps. First, a non-equilibrium distribution of electron-hole pairs is created by means of light, heat or injection of excess carriers. Photoluminescence (PL) is the method of exciting electron-hole pairs by photons with energy higher than the band gap E_g. Second, electrons and holes respectively reach a quasi-thermal equilibrium in a time much shorter compared to that of recombination. So we can obtain information of electronic band structures of semiconductors no matter which method is used for excitation. Finally, the electron-hole pairs recombine radiatively. There are several radiative processes in luminescence, including band-to-band transitions, free-to-bound transitions and donor-acceptor pair transitions.

Excess electrons and holes also can recombine nonradiatively, such as a multiphonon process and Auger process. Those non-radiative processes lower the quantum efficiency and

make luminescence hard to detect. Because of the large dielectric constant and very small effective masses of electrons and holes of lead sulfide, the binding energy of impurities is negligible and electron-hole pairs can be thermally excited from the localization of impurities even at low temperature. For relatively pure samples like the lead sulfide samples used in our experiments, when the concentration of impurities is relatively low, luminescence is only contributed by band-to-band transitions.

2.2.2 Band-to-Band Transitions

Band-to-band transitions involve the recombination of free electrons in the conduction band with free holes in the valence band [10]. From the principle of detailed balance, the rate of absorption and rate of emission equal each other at the thermal equilibrium. Under certain conditions, the photoluminescence intensity $I(\omega)$ is related to the absorption coefficient $\alpha(\omega)$ by [10]:

$$\boxed{I(\omega) = C\alpha(\omega)exp\left(-\frac{\hbar\omega - E_g}{k_B T}\right)} \tag{2.11}$$

Where C is a constant. So photoluminescence spectra start when the energy increases over the band gap E_g. The peak is usually broad and asymmetric, with a tail at the high energy end.

2.3 Temperature and Isotopic Mass Dependence of the Band Gap in Semiconductors

The band gap of semiconductors varies with temperature as well as with the isotopic masses of the atoms through the electron-phonon interaction at constant pressure [3]. Under the adiabatic approximation, the electronic band structure is mainly determined from the rough model that a free electron gas interacts with the periodic potentials of fixed ion cores. The band structure is modified to first order by the interaction of the electrons and the slight vibration of the ion cores around their equilibrium positions, namely the electron-phonon interaction. The electron-phonon interaction is dependent on the averaged squared phonon amplitude, which is a function of temperature and atom masses. The former gives a description of the average degree of motion of the ion cores and the latter is a measure of the inertia of the ion cores against changes of motion.

2.3.1 General Relations

The dependence of the band gap E_g on the temperature T at constant pressure P can be divided into two contributions [12] [13]. (The dependence of the band gap on isotopic masses shares the same relation described by Formula (2.12), but it has the derivative with respect to isotopic masses in each term.)

$$\left(\frac{\partial E_g}{\partial T}\right)_P = \left(\frac{\partial E_g}{\partial T}\right)_{EP} + \left(\frac{\partial E_g}{\partial T}\right)_{ThermalExp} \tag{2.12}$$

The first term on the right hand side of (2.12) represents the "explicit" electron-phonon interaction at constant volume V, while the second term is due to the change of the lattice constant or the change of the crystal volume with T. It originates from the anharmonic term in the expansion of the vibration of the ion cores around the equilibrium positions, which corresponds to the thermal expansion of materials. Hence we call it the thermal expansion term.

The thermal expansion term can be further be written as: .

$$\begin{aligned}\left(\frac{\partial E_g}{\partial T}\right)_{ThermalExp} &= -\left(\frac{\partial E_g}{\partial P}\right)_T \left(\frac{\partial P}{\partial lnV}\right)_T \left(\frac{\partial lnV}{\partial T}\right)_P \\ &= -3\alpha B \left(\frac{\partial E_g}{\partial P}\right)_T \end{aligned} \tag{2.13}$$

where α is the linear thermal expansion coefficient, $B = (\partial P/\partial lnV)_T$ is the bulk modulus and $(\partial E_g/\partial P)_T$ is the pressure dependence of the band gap at constant temperature. Those parameters are available for most semiconductors in semiconductor handbooks and hence the thermal expansion term can be calculated numerically.

To evaluate the effect of the "explicit" electron-phonon interaction on the band gap, the energy band $E_n(k)$ with branch n and at the point k in the reciprocal space can be written as the sum of the unperturbed energy $\epsilon_n(k)$ and a perturbation [14]:

$$E_n(k) = \epsilon_n(k) + \sum_{j,q} \left(\frac{\partial E_n(k)}{\partial n_{j,q}}\right)\left(n_{j,q} + \frac{1}{2}\right) \tag{2.14}$$

where $n_{j,q}$ is the occupation number of the phonons with branch j and at the point q. It is a Bose-Einstein factor $\left[1/\left(e^{\hbar\omega/k_BT} - 1\right)\right]$ under thermal equilibrium conditions. The coefficient $(\partial E_n(k)/\partial n_{j,q})$ is the sum of a Debye-Waller term and the real part of the self-energy. The former term is the simultaneous interaction of an electron and two phonons

with the same wave vector q and from the same branch j, or second-order electron-phonon interaction taken in first-order perturbation theory; while the latter term results from the electron-one-phonon interaction taken to second-order perturbation theory [13].

The normalization of the band gap energy, or the total change of the band gap energy as a function of temperature T as well as isotopic masses M is the sum of respective perturbations of the valence and conduction bands:

$$E_g(T, M) = E_C(k) - E_V(k) \tag{2.15}$$

$E_g(T, M)$ could be theoretically calculated if a good pseudopotential description of the electronic band structure and a good lattice dynamical model were available. Even at $T = 0$, there is a change of the band gap due to the zero-point vibration and we call it the zero-point renormalization of the band gap. In the following, we build up the simplified models to understand the experimental data of the band-gap shift induced by both temperature and isotopic masses and measure the zero-point renormalization of the band gap.

2.3.2 Simplified Models

We now simplify the electron-phonon interaction coefficients in (2.14) by making two assumptions [14]. First, instead of summing over all possible phonon modes by using the complete phonon dispersion, we pick a few averaged phonons determined by the phonon density of states (Bose-Einstein model). Second, in order to avoid the complicated calculation of the coefficients $(\partial E_n(k)/\partial n_{j,q})$, which becomes more difficult for semiconductors whose electronic band structure and lattice dynamics can not be described in simple models, we approximate those coefficients by the effective electron-phonon coupling coefficients A_i. The above simplifications lead to the expression:

$$E_g(T, M) = E_{g0} + \sum_i \frac{A_i}{\omega_i M_i} \left[n\left(\omega_i, T\right) + \frac{1}{2} \right] \tag{2.16}$$

where E_{g0} is the unrenormalized band gap energy. ω_i is the average phonon energy (in K, the same units as temperature T) and M_i is the reduced mass for the vibration mode corresponding to ω_i.

The derivative of $E_g(T, M)$ with respect to isotopic masses M_i is:

$$\begin{aligned}\frac{\partial E_g(T,M)}{\partial M_i} &= \frac{\partial\left[\frac{A_i}{\omega_i M_i}\left[n\left(\omega_i, T\right)+\frac{1}{2}\right]\right]}{\partial M_i} \\ &= \frac{A_i}{\omega_i M_i}\frac{\partial n\left(\omega_i, T\right)}{\partial M_i}+A_i\left[n\left(\omega_i, T\right)+\frac{1}{2}\right]\frac{\partial\left[\frac{1}{\omega_i M_i}\right]}{\partial M_i} \end{aligned} \tag{2.17}$$

The first part of (2.17) has almost no contribution in the low temperature limit. Taking into account the proportionality of $\omega_i \sim M_i^{-1/2}$ [15], we find the isotope shift per atomic mass unit in the limit $T \rightarrow 0$ to be:

$$\frac{\partial E_g(T=0,M)}{\partial M_i} = -\frac{A_i}{4\omega_i M_i^2} \tag{2.18}$$

Bringing (2.18) back into (2.16), we finally obtain the practical expression for the fitting of experimental data:

$$\boxed{E_g(T,M) = E_{g0} - \sum_i 4M_i \frac{\partial E_g(T=0,M)}{\partial M_i}\left[n\left(\omega_i, T\right)+\frac{1}{2}\right]} \tag{2.19}$$

where the zero-point renormalization of the band gap is given by $[-\sum_i 2M_i\left(\partial E_g/\partial M_i\right)]$. Henceforth, the isotope shift per atomic mass unit $(\partial E_g(T=0,M)/\partial M_i)$ will be abbreviated as $(\partial E_g/\partial M_i)$.

The choice of the number of oscillators is material-specific [2]. A one-oscillator description is good enough for most semiconductors, especially elements of group IV. However it is necessary to use a two-oscillator model for binary compounds in which cation and anion have very different masses. One of them represents the acoustic mode dominated by the heavier atoms and the other is from the optical mode dominated by the lighter atoms. There is much improvement in the fitting especially when the isotope shift per atomic mass unit turns out with opposite sign. (Generally there are different isotopic mass dependences corresponding to different atomic masses in semiconductor compounds. Under some circumstances, even with opposite signs [6].) For compounds where cation and anion contributions almost cancel each other, a three-oscillator model would be applied, corresponding to transverse acoustic (TA), longitudinal acoustic (LA) and longitudinal optical (LO) phonons. It is proven that additional oscillators do not improve the accuracy significantly.

There are drawbacks on the Bose-Einstein model. The model can not reproduce a T^4 dependence of the band-gap shift at a very low temperature, typically in the region

$T < 0.01\ \theta_D$ or $T < 5$ K [16]. (The Debye temperature θ_D is below 450 K for most materials; 225 K for lead sulfide.)

We end with a fully phenomenological expression for fitting the temperature dependence of the band gap. A widely accepted one, proposed by Pässler [11], is:

$$\boxed{E_g(T) = E_g(0) - \frac{\alpha\Theta_p}{2}\left[\sqrt[p]{1+\left(\frac{2T}{\Theta_p}\right)^p} - 1\right]} \tag{2.20}$$

Θ_p is roughly understood as the average phonon energy, in units of temperature. For high enough T, the expression gives a linear dependence of the band gap on temperature and α gives the slope at $T \to \infty$. The availability of experimental data $E_g(T)$ up to the vicinity of the Debye temperature in a given material is found to be a necessary condition for trustworthy determinations of the limiting slopes of the $E_g(T)$ curves in the high temperature region. At very low T, the expression yields:

$$E_g(T) \approx E_g(0) - \frac{\alpha\Theta_p}{2p}\left(\frac{2T}{\Theta_p}\right)^p \tag{2.21}$$

where p gives the index of the temperature power law of the band gap for $T \to 0$ or $T \ll \Theta_D$. The value for most materials lies within $2 \leq p \leq 3.3$ and a little lower than the expected theoretical value 4. The resulting zero-point renormalization of E_g is:

$$\triangle_g(0) = -\frac{\alpha\Theta_p}{2} \tag{2.22}$$

Depending on the dispersion of phonon energy spectra, we can choose the most appropriate models for different regimes. (The qualitative description of different regions is introduced in [11].) For the regime of small dispersion, the contribution of low energy phonons is very small in comparison with that of high energy phonons. The corresponding band gap $E_g(T)$ shows a very weak dependence (tending to be a plateau behavior) in the cryogenic region and can be described in reasonable approximation by the Bose-Einstein model. In the regime of intermediate dispersion, the simple analytic four-parameter expression is capable of providing fine numerical fittings with physically reasonable estimation of parameters for most group IV, III-V and II-VI materials.

Chapter 3

Experimental Method

In this chapter, we go through the details of the experimental setup for both photoluminescence and infrared absorption spectroscopies. Because of the similarities between them, we treat them together instead of one by one. Because of the importance and complexity of Fourier transform spectrometry and the continuous flow, variable temperature cryostat, we discuss them at first and then go through the other parts. We end the chapter with the sample preparation.

3.1 Fourier Transform Spectrometry

Spectrometry is the detection, measurement and analysis of electromagnetic radiation as a function of photon energy [17] [18]. The essential problem of spectrometry is the measurement of the intensity of radiation as a function of frequency (equivalently wavenumber in the units of cm^{-1} in this thesis).

Dispersive spectrometers, such as diffraction gratings, acquire the spectrum by spatially separating radiation with different frequencies. Fourier transform spectrometry (FTS is used as the abbreviation of either Fourier transform spectrometry or Fourier transform spectrometer, as the context requires), is a method of obtaining high resolution spectra in a broad region simultaneously. The term FTS originates from the fact that incoming radiation and outgoing radiation are related to each other by a Fourier transform. This kind of spectrometer is realized by using a scanning Michelson interferometer to transform the incoming radiation into an amplitude-modulated signal. These modulation frequencies are detected and recorded as an interferogram (intensity distribution in terms of optical path

difference). By taking the Fourier transform of the interferogram, the original spectrum of incoming radiation is accurately recovered.

Fourier transform spectrometry has many merits compared to traditional dispersive spectrometry. First, FTS can achieve a much higher resolution (0.004 cm^{-1} for our BOMEM DA8 system with a 2.5 m long scanning tube, typically two orders of magnitude higher than that of diffraction gratings), giving better estimates of spectral line positions, intensities, line shapes and areas. Second, FTS can take a broad spectral region simultaneously, whereas dispersive spectrometers' collection time increases linearly with the spectral width. Generally FTS is the system of choice in the infrared region under almost any conditions and in the visible and ultraviolet regions when high spectral resolution is required.

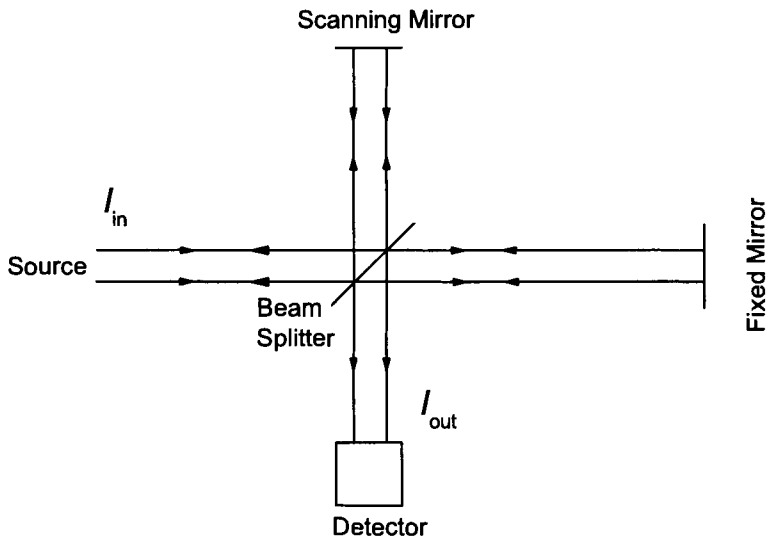

Figure 3.1: Schematic diagram of a Fourier transform spectrometer.

A typical Fourier transform spectrometer is in principle a Michelson interferometer (Figure 3.1). The input radiation from the source is collimated into a beam splitter, which divides the beam into two equal parts, one transmitted and one reflected. After the two beams travel separately through the two arms of the interferometer, they recombine into one and are recorded by the detector.

Assume the input radiation goes with the frequency dependence of power intensity [19]:

$$dI_{in} = B(\sigma)d\sigma \tag{3.1}$$

where $B(\sigma)$ is the power spectral density of the input radiation at the frequency interval $d\sigma$ and corresponds to the desired measurement. Then the interferogram recorded by the detector can be expressed as:

$$I_{out}(x) = \frac{I_{in}}{2} + \int_{-\infty}^{+\infty} \frac{B(\sigma)}{2} \cos(2\pi\sigma x)d\sigma \tag{3.2}$$

where x (in units of cm) is the optical path difference of the Michelson interferometer, which is twice the displacement of the scanning mirror. Taking an inverse cosine Fourier transform of (3.2) we then can express $B(\sigma)$ as:

$$B(\sigma) = 2\int_{-\infty}^{+\infty} \left(I_{out}(x) - \frac{I_{in}}{2}\right) \cos(2\pi\sigma x)dx \tag{3.3}$$

The optical path difference x can not reach infinity in a practical instrument. I_{in}, which is constant when x changes, has essentially zero contribution to the integral in a finite space, and can be neglected compared to the integral of the first term. We then reach the practical formula:

$$\boxed{B(\sigma) = 2\int_{finite} I_{out}(x) \cos(2\pi\sigma x)dx} \tag{3.4}$$

The resolution of a Fourier transform spectrometer is characterized by the full width at half maximum (FWHM) of a peak. It is mainly limited by the finite optical path difference x:

$$FWHM = 1.207\left(\frac{1}{x}\right) \tag{3.5}$$

For the scanning mirror with a maximum travelling distance of 250 cm in our lab, x is 500 cm and the maximum possible resolution is 0.0024 cm^{-1}. When additional factors are considered, such as the apodization function used in computing the spectrum, the divergence of the beam passing through the interferometer and the stability of the mirror drive system and laser, we can reproducibly reach 0.004 cm^{-1} [19].

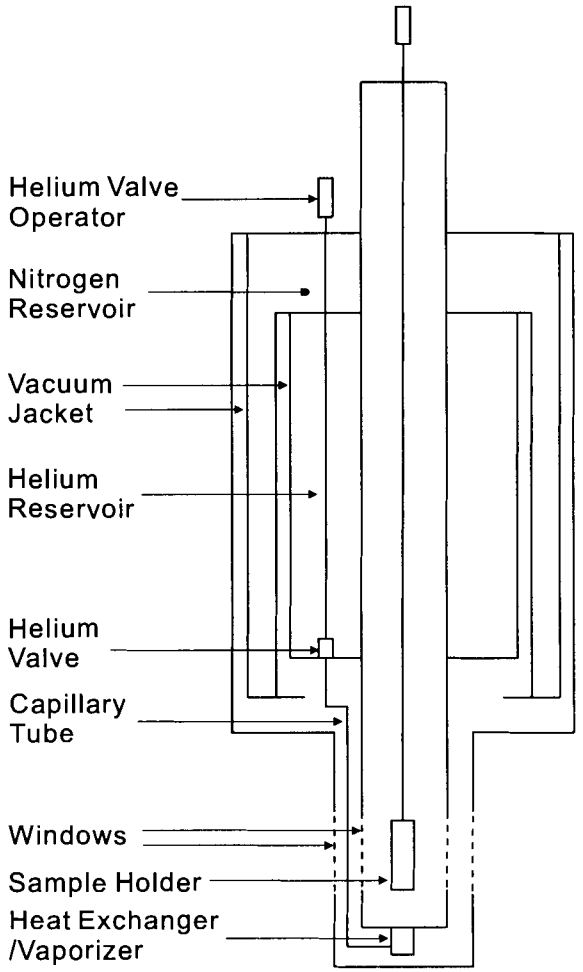

Figure 3.2: Schematic diagram of the continuous flow, variable temperature cryostat.

3.2 Continuous Flow, Variable Temperature Cryostat

A cryostat, an essential part of cryogenics, is a very efficient thermal barrier between the ultralow temperature cryogenic environment and the room temperature environment [22]. A continuous flow, variable temperature cryostat from Janis Research Company was used for the experiments (Figure 3.2). It is composed of three chambers thermally isolated from one another. The outer one is the nitrogen reservoir, which pre-cools the dewar at liquid nitrogen temperature 77 K. The helium reservoir, which is the middle one, is isolated from room temperature by the outer one and can last up to 10 hours at 4.2 K when it is

fully filled with liquid helium. Samples can be observed through the bottom window in the sample chamber (the inner chamber). The window made of Zinc Selenide (ZnSe) was chosen to reduce absorption in the mid-infrared region. The design of the detachable tail helps integrate the cryostat to the spectrometer. A helium valve which is located at the bottom of the helium reservoir, is connected to a heat exchanger/vaporizer at the bottom of the sample chamber via a capillary tube. We can channel liquid helium from the helium reservoir to the heat exchanger by the helium valve. At that point, little heat may be added to vaporize the liquid helium (liquid helium has a very low latent heat of vaporization) and vary its temperature from 4.2 K up to 320 K. The helium vapor flows up the sample chamber and determines the temperature of the samples attached to the sample holder. We also can reach a temperature as low as 1.6 K by reducing the pressure of the helium vapor. Hence, the temperature of the samples can be controlled by both the helium valve operator and the heater at the bottom of the sample chamber and real-time monitored by a temperature sensor close to the sample.

Heating samples by helium flow has many advantages compared to heating samples in thermal contact with the temperature-controlled sample holder. We avoid a thermal gradient error between the sample and the sample holder, obtain the more accurate measurement of the sample's temperature and save much helium when vacuuming the sample chamber to reduce the temperature below 4.2 K. The temperature stability of the sample is usually better than 0.1 K in the range 4.2 K to 25 K.

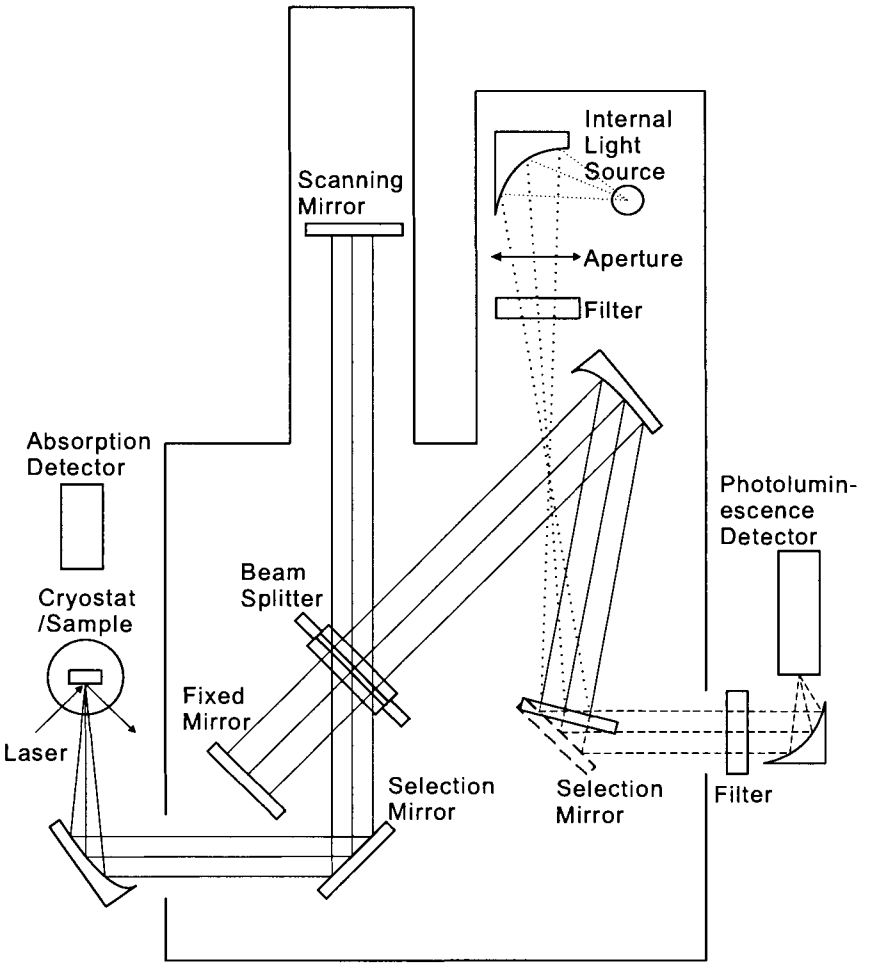

Figure 3.3: Schematic diagram of the experimental setup for both photoluminescence and infrared absorption spectroscopies. The optical paths are indicated by dashed lines (only for photoluminescence), dotted lines (only for infrared absorption) and solid lines (shared for both).

3.3 Experimental Setup

The experimental setup for both photoluminescence and infrared absorption spectroscopies consists of a sample, a cryostat, an excitation source, a spectrometer and a radiation detector. Also the assorted optical and electronic instruments are needed.

In the experimental setup for photoluminescence spectroscopy, the samples were

mounted in a strain-free manner and immersed in liquid helium. The helium vapor pressure was pumped down by a mechanical pump and we can reach a temperature as low as 1.6 K. By reducing the helium temperature below the point of superfluidity (2.18 K at 38.5 mm mercury pressure), liquid helium transits to the bubble-free superfluid phase and gives a higher signal-to-noise ratio. Also the near-zero temperature condition eliminates various spontaneous excitations which are irrelevant to our research. The samples were excited on the front face by a multiline argon ion laser and the induced luminescence was collimated by a parabolic mirror and then directed into the Fourier transform spectrometer BOMEM DA8. A CaF_2 beam splitter (10 cm diameter, coated with Sb_2S_3 and working in the optical range $1,200 \sim 10,000$ cm^{-1} [20]) and a liquid nitrogen cooled InSb detector (1 mm^2 area and working in the optical range $1,800 \sim 8,500$ cm^{-1} [21]) were chosen for the mid-infrared region. A 1038 nm long pass filter was used to cut out the argon ion laser signal.

The only differences between the experimental setup for infrared absorption spectroscopy compared to photoluminescence, are the sample setup and the light source. The samples were mounted inside a Model KRS-5 cryostat, a continuous flow, variable temperature cryostat from Janis Research Company. The temperature of the samples, varying from 1.6 K to 320 K, can be controlled and real-time monitored by an automatic temperature controller (Model 330 from Lakeshore Company). The internal light sources of the BOMEM DA8, a Globar source and a Quartz lamp, both with continuous, broad spectrum covering the mid-infrared region, are chosen. Accordingly there are changes of the optical paths in the BOMEM DA8.

3.4 Sample Preparation

Three types of samples with different isotopic composition of sulfur were provided by our collaborators M. Cardona and R. Lauck at the Max-Planck-Institut für Festkörperforschung in Stuttgart, Germany. (There are relatively large isotope effects in sulfur compared to that of lead because of the relatively small mass of sulfur.) Natural lead sulfide bulk single crystals with an abundance of about 95% ^{32}S are from the minerals in Creede, Colorado, USA. We can regard natural samples as almost monoisotopic because of the dominance of ^{32}S. Synthetic crystals with the natural abundance of ^{32}S were used as reference samples for the PL study. We also studied synthetic isotopic samples with an abundance of 99% of ^{34}S.

Pb^{34}S and the natural PbS reference samples were grown by sublimation at $800° \sim 875°$

Celsius in an argon atmosphere of 150 mbar, under an excess of sulfur ($5 \sim 40$ mbar) provided by a sulfur reservoir. In this manner, the growth of a larger main crystal close to the PbS source was favored. Such crystals exhibit a (100) face of about 1×1 mm^2 in area with macroscopic (0.1 mm) steps.

The three samples are all p-type and have hole concentrations of 2×10^{17} cm^{-3}, 1.7×10^{18} cm^{-3} and 9×10^{18} cm^{-3} respectively. The types and carrier concentrations were separately determined by the sign of the Seeback effect and infrared reflectivity in a recent study of the Raman spectra of the same samples [23].

The desired thickness of natural PbS for high signal-to-noise ratio absorption edge measurements is roughly estimated. For the Globar source, which is used in the experiments, the recorded maximum intensity of reference light in the PbS absorption edge is ~ 2000 AU (Arbitrary Unit) and we assume the reliable minimum is ~ 0.2 AU. Those give the minimum ratio of intensity of transmitted light to that of reference light $\sim 10^{-4}$. On the other hand, the absorption coefficient of lead sulfide abruptly increases from ~ 0 cm^{-1} to 10^4 cm^{-1} in the absorption edge region. If we want to reach absorption coefficients as high as 1000 cm^{-1}, the thickness of the samples should be thinner than $\left[-\ln\left(10^{-4}\right)/1000 \approx 69\ \mu\text{m}\right]$. PbS crystals are of fragile nature and it is difficult to prepare these super thin samples. We managed to grind and polish the natural sample down to 45 μm. The actual thickness of the samples is calculated from the interference fringe pattern of the transmission spectrum.

Chapter 4

Results and Discussion

4.1 Sulfur Isotope Shift Using Photoluminescence Spectroscopy

We took photoluminescence measurements of lead sulfide samples at a temperature of 1.6 K. Because of their high similarity, the synthetic $Pb^{nat}S$ and $Pb^{34}S$ samples were used to illustrate the small isotope shift.

Figure 4.1 shows a typical photoluminescence spectrum of the lead sulfide samples grown using natural S at low temperature. The peak corresponds to the transition of free carriers from the conduction band to the valence band. In principle, by fitting the peak by the intensity of the photoluminescence formula for band-to-band transitions (2.11), we can determine the band gap, although we only care about the relative shift of the peaks. The broad shoulder near the low energy end is from the background blackbody radiation at room temperature, which becomes increasingly obvious when we lower the excitation intensity.

Figure 4.2 illustrates the isotope shift of band-to-band transitions between synthetic $Pb^{nat}S$ and $Pb^{34}S$ in photoluminescence spectra. The peaks of different samples are scaled to the same height, so we can easily observe and measure the isotope shift. The peaks of $Pb^{nat}S$ (solid line) and $Pb^{34}S$ (dashed line) have very similar shapes, and the slight difference in shape is possibly from the broadening due to the isotopic disorder of sulfur [1] or the band-tail states induced by the different concentrations of impurities. The direction of the isotope shift is abnormal compared to most materials. The energy is seen to decrease with increasing isotopic mass of sulfur. The measured shift is 7 ± 2 cm^{-1}, or 0.87 ± 0.25

meV. The error bar is estimated partly from the resolution of photoluminescence spectra 0.5 cm^{-1} and partly from the mismatch of the shapes of the two peaks. This shift gives the sulfur isotope shift per atomic mass unit:

$$\frac{\partial E_g}{\partial M_S} = \frac{7 \pm 2}{32 - 34} \times 0.124 = -0.43 \pm 0.12 \text{ meV/amu} \tag{4.1}$$

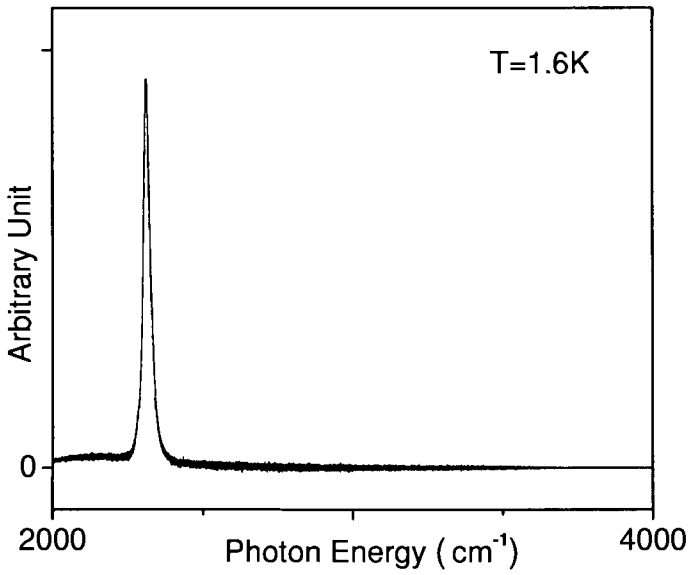

Figure 4.1: Photoluminescence spectrum of synthetic $Pb^{nat}S$ at a temperature of 1.6 K. The peak corresponds to the band-to-band transitions of free carriers and the broad shoulder near the low energy end is from the background blackbody radiation at room temperature.

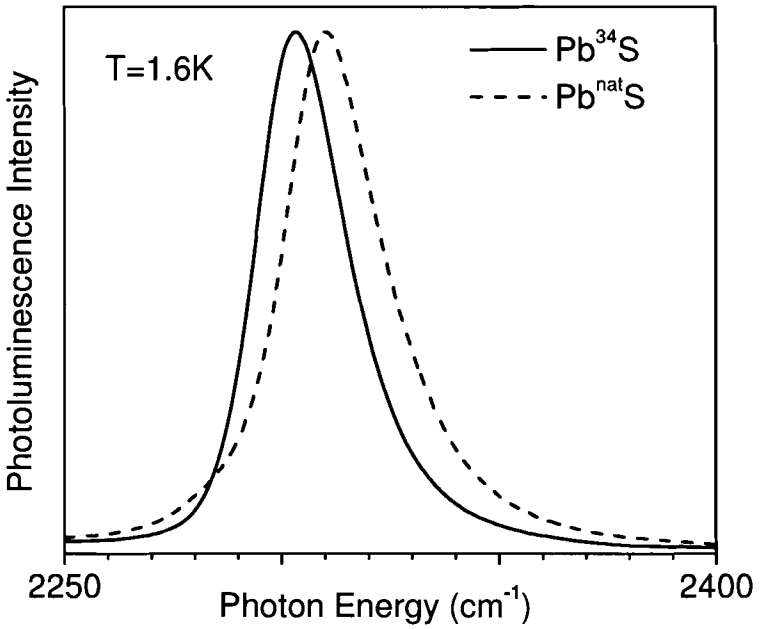

Figure 4.2: Isotope shift of band-to-band transitions between synthetic $Pb^{nat}S$ and $Pb^{34}S$ in photoluminescence spectra with a resolution of 0.5 cm^{-1}. The peaks of different samples are scaled to the same height, so we can easily observe and measure the isotope shift. The measured value of the shift is 7 ± 2 cm^{-1}, or 0.87 ± 0.25 meV.

4.2 Zero-Point Renormalization of the Band Gap Using Infrared Absorption Spectroscopy

4.2.1 Results

We took infrared absorption measurements of the high quality natural Creede samples at a given temperature. Only the natural Creede samples are large enough for the measurements. The absorbance spectrum is calculated from $[-\ln(transmitted\ spectrum/reference\ spectrum)]$. The absorbance is related to the absorption coefficient by a factor of the thickness of the samples. We can treat them equally given that the sample thickness is a constant, which is satisfied when the thickness is almost

uniform and the light spot incident on the sample is small (around 2.5 mm in diameter).

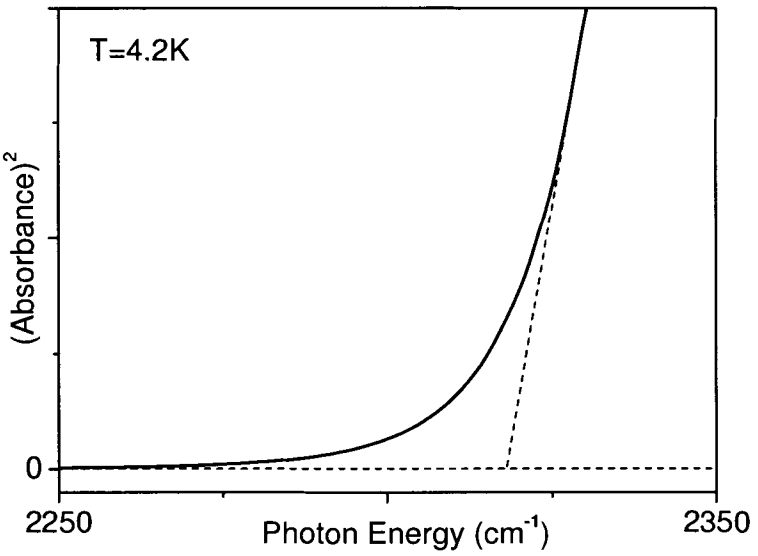

Figure 4.3: Squared absorbance spectrum of the natural Creede PbS sample in the absorption edge region at a temperature of 4.2 K (solid line). The absorbance curve is fitted by a straight line (dashed line) and the intercept with the horizontal line of zero absorption coefficient (dashed line) gives the band gap.

Figure 4.3 shows a typical squared absorbance spectrum [24]. Qualitatively the squared absorbance spectrum of the natural Creede PbS sample around the band gap region at a temperature of 4.2 K (solid line) agrees well with the theory introduced in Section 2.1. Below the band gap, the absorption coefficients remain zero. Above the threshold value, the absorption coefficients go up abruptly. Quantitatively, based on the absorption formula for direct and allowed transitions in the absorption edge (2.9), a strict straight line should show up starting from the band gap. The excess absorption at low energy may result from band-tail states induced by impurities. When the photon energy is continuously increased, the absorption coefficient shows the expected shape and can be fitted by a straight line (dashed line). The intercept with the horizontal line of zero absorption coefficient (dashed

line) gives the band gap. The error of estimating the band gap, 5 cm^{-1} or 0.6 meV, is partly from the resolution of the absorption measurements 2.5 cm^{-1} and partly from the error of estimating the best fitting line. However, the difference in band gap between two nearby temperatures can be determined with much higher precision. When the temperature increases, the whole structure shifts towards the high energy end and the slope of the fitting line decreases gradually, which gives a higher band gap energy.

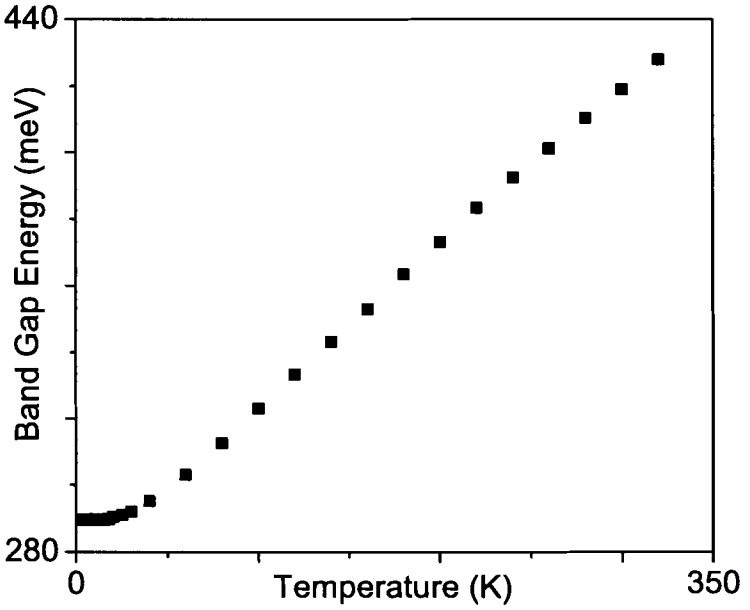

Figure 4.4: Total temperature dependence of the band gap of natural Creede PbS from 1.6 K to 320 K.

We varied the temperature from 1.6 K through 320 K to obtain the total temperature dependence of the band gap. Multiple measurements were made to achieve the most accurate results so far. First, we did the measurements of the 100μm thick samples twice, in consecutive days. The data was perfectly reproducible. Then we polished the samples down to 45μm and again the data was well reproduced. Considering that the thinner samples allow us to measure absorption coefficients over a wide energy range (Section 3.4) and thus

obtain a better straight-line relation above the band gap, we chose the latter data as the standard data.

Figure 4.4 shows a few features. Below 15 K, we can not observe any change of the band gap within our error bar although we set up experimental points every 2.5 K. The 15 K to 30 K region shows the first bend of the curve where the band gap gradually increases with increasing temperature. Hence more experimental points were measured in this region to estimate the bend shape. Starting from 30 K, the temperature dependence of the band gap is almost a straight line except for another subtle bend downwards around 170 K.

4.2.2 Discussion

We firstly fit the temperature dependence of the band gap to the Pässler empirical formula (2.20).

In general, the empirical expression gives a good description of the change of the band gap with temperature (Figure 4.5). It exactly reproduces the first bend around 20 K and the straight line above 30 K. However, the second bend around 170 K can not be simulated. Also the slope of the fitting line does not bend downward at the high energy end.

The fitting gives the unperturbed $T = 0$ band gap $E_g(0) = 289.5$ meV and the average phonon temperature $\Theta_p = 59$ K. The slope of the fitting line at $T \rightarrow \infty$, α, is 0.48 meV/K, having a reasonable magnitude and showing the abnormal response to temperature compared to most materials. p is relatively high, 5.1 compared with the intermediate region $2 \leq p \leq 3.3$, showing that there is a large dispersion of the phonon energy spectrum and indicating that a better fitting might be obtained with the Bose-Einstein model (Section 2.3.2). The total zero-point renormalization of the band gap is given as:

$$\triangle_g(0) = -\frac{\alpha\Theta_p}{2} = -14.4 \text{ meV} \tag{4.2}$$

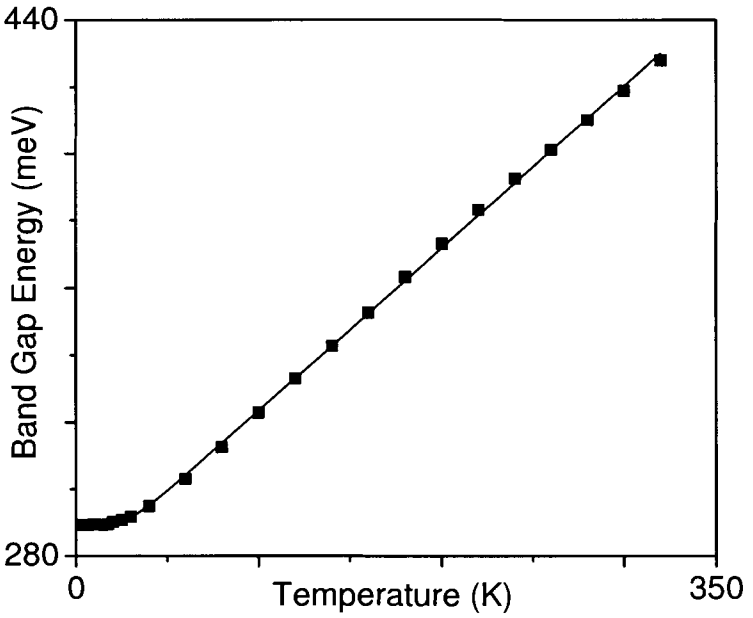

Figure 4.5: Fitting of the temperature dependence of the band gap with the Pässler empirical formula (2.20). The experimental data is shown by solid squares and the fitting is shown by a solid line.

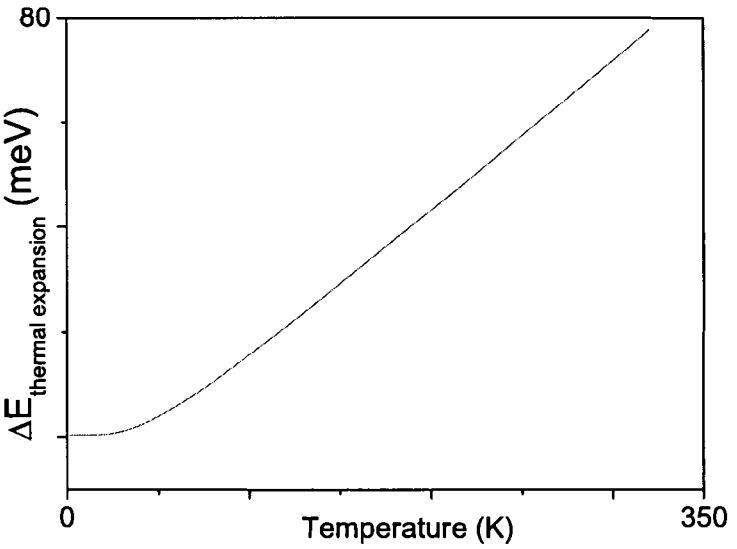

Figure 4.6: Change of the band gap due to the thermal expansion. The curve shows one-oscillator Bose-Einstein model fitting (solid line) to the available data on the thermal expansion coefficient [29]).

We can estimate the change of the band gap due to the thermal expansion based on (2.13) [25]. The respective values for lead sulfide found in the literature are bulk modulus $B = 50$ GPa at 295 K [26] and the pressure derivative at 295 K $(\partial E_g/\partial P)_T = -9.1 \times 10^{-6}$ eV/bar [27]. The negative product of the two values gives the deformation potential of the band gap 4.5 eV [28]. The linear thermal expansion coefficients of lead sulfide above 30 K can be found in the literature [29] and we extrapolate the curve down to 1.6 K. Multiplying the integral of the linear thermal expansion coefficients by 3 gives the thermal expansion in volume. Hence we finally reach the band gap due to the thermal expansion shown in Figure 4.6.

Two abnormal features are shown in Figure 4.6. The thermal expansion has the same effect on the band gap as the net electron-phonon interaction. Also the thermal expansion contributes about half of the change of the band gap. Given by the one-oscillator Bose-Einstein model fitting, the zero-point renormalization of the band gap due to the volume change is 17.0 meV.

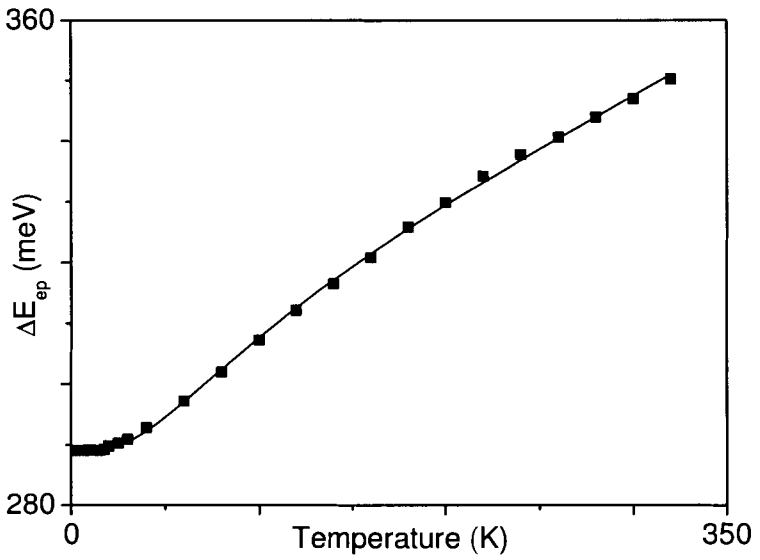

Figure 4.7: Change of the band gap due to the net electron-phonon interaction (raw data minus the thermal expansion contribution). The curve shows the three-oscillator Bose-Einstein model fitting to the experimental data (solid square).

Subtracting the thermal expansion effect (Figure 4.6) from the raw data (Figure 4.5), we obtain the change of the band gap due to the net electron-phonon interaction (Figure 4.7). A three-oscillator Bose-Einstein model is applied for the fitting. The frequencies of the three discrete oscillators are 50 cm^{-1} mainly from lead vibrations, 93 cm^{-1} from the transverse optical (TO) phonon of sulfur and 225 cm^{-1} from the longitudinal optical (LO) phonon of sulfur [30] [31]. It is shown that the fitting is not perfect but reproduces the two bends well. The zero-point renormalization of the band gap due to the net electron-phonon interaction is -17.7 ± 4.6 meV. So the total renormalization of the band gap is ~ 0 meV, possibly due to an almost complete cancellation between the cation and anion contributions. As discussed in Section 2.3, we believe that the value from the 3 oscillator Bose-Einstein model is more reliable than the -14.4 meV given by the fit using the Pässler model. The lead isotope shift in lead sulfide is estimated from (2.19): $(0 + 2 \times 33 \times 0.43)/(2 \times 207) = 0.069$ meV/amu.

In conclusion, sulfur has a strong "negative" isotope effect on the band gap of PbS. The

measured value is 0.43 ± 0.13 meV/amu. Because of the large atomic mass of lead, the direct measurement of the isotope effect for lead has not yet been possible. We also report improved measurements of the temperature dependence of the band gap of PbS. The total zero-point renormalization of the band gap is ~ 0 meV, which indicates that lead has the opposite effect on the band gap compared with sulfur. The predicted value of the isotope shift per atomic mass unit for lead is 0.069 meV/amu.

Results of the isotope effects on the fundamental band gap in lead sulfide are summarized in Table 4.1:

	$E_g(T \approx 0)$ meV	$\partial E_g/\partial M_{Pb}$ meV/amu	$\partial E_g/\partial M_S$ meV/amu	$\Delta E_g(T=0)$ meV	$(\partial E_g/\partial T)_{T\to\infty}$ meV/K
PbS	289.4 ± 0.6	0.069	-0.43 ± 0.12	~ 0	0.45

Table 4.1: Summary of isotope effects on the fundamental band gap of lead sulfide. The columns from left to right are: the band gap at the lowest temperature, the predicted cation isotope shift per atomic mass unit, the measured anion isotope shift per atomic mass unit, the total renormalization of the band gap at $T = 0$ and the linear T-coefficient of $E_g(T)$ in the high T-limit.

Bibliography

[1] M. Cardona and M. L. W. Thewalt. Isotope Effects on the Optical Spectra of Semiconductors. To be published.

[2] M. Cardona. Electron-Phonon Interaction in Tetrahedral Semiconductors. *Solid State Commun.*, 133:3, 2005.

[3] A. K. Ramdas, S. Rodriguez, S. Tsoi, and E. E. Haller. Electronic Band Gaps of Semiconductors as Influenced by Their Isotopic Composition. *Solid State Commun.*, 133:709, 2005.

[4] R. Dalven. A Review of the Semiconductor Properties of PbTe, PbSe, PbS and PbO. *Infrared Phys.*, 9:141, 1969.

[5] Y. I. Ravich, B. A. Efimova, and I. A. Smirnov. *Semiconducting Lead Chalcogenides.* Plenum Press: New York, London, 1970.

[6] N. W. Ashcroft and N. D. Mermin. *Solid State Physics.* Holt, Rinehart and Winston: New York, 1976.

[7] G. Nimtz and B. Schlicht. *Narrow-Gap Semiconductors*, volume 98 of *Springer Tracts in Modern Physics.* Springer-Verlag: Berlin, New York, 1983.

[8] P. Y. Yu and M. Cardona. *Fundamentals of Semiconductors: Physics and Materials Properties*, third edition. Springer-Verlag: Berlin, New York, 2001.

[9] H. Kuzmany. *Solid State Spectroscopy: An Introduction.* Springer-Verlag: Berlin, New York, 1998.

[10] D. Dragoman and M. Dragoman. *Optical Characterization of Solids.* Springer-Verlag: Berlin, New York, 2002.

[11] R. Pässler. Parameter Sets due to Fittings of the Temperature Dependencies of Fundamental Bandgaps in Semiconductors. *Phys. Stat. Sol. (b)*, 216:975, 1999.

[12] N. Garro, A. Cantarero, M. Cardona, A. Göbel, T. Ruf, and K. Eberl. Dependence of the Lattice Parameters and the Energy Gap of Zine-Blende-Type Semiconductors on Isotopic Masses. *Phys. Rev. B*, 54:4732, 1996.

[13] S. Zollner, M. Cardona, and S. Gopalan. Isotope and Temperature Shifts of Direct and Indirect Band Gaps in Diamond-Type Semiconductors. *Phys. Rev. B*, 45:3376, 1992.

[14] A. Göbel, T. Ruf, M. Cardona, C. T. Lin, J. Wrzesinski, M. Steube, and K. Reimann. Effects of the Isotopic Composition on the Fundamental Gap of CuCl. *Phys. Rev. B*, 57:15183, 1998.

[15] M. Cardona. *Phys. Stat. Sol. (b)*, 220:5, 2000.

[16] M. Cardona, T. A. Meyer, and M. L. W. Thewalt. Temperature Dependence of the Energy Band Gap of Semiconductors in the Low-Temperature Limit. *Phys. Rev. Lett.*, 92:196403, 2004.

[17] S. P. Davis, M. C. Abrams, and J. W. Brault. *Fourier Transform Spectrometry.* Academic: San Diego, 2001.

[18] S. Johnston. *Fourier Transform Infrared: a Constantly Evolving Technology.* E. Honwood: New York, 1991.

[19] *Spectrometer System Manual*, revision 3.1. Bomem Inc., 1990.

[20] *Beamsplitter User's Guide*, revision 1.2. Bomem Inc.

[21] *DA Series Detectors Manual*, revision preliminary. Bomem Inc., 1989.

[22] M. N. Jirmanus. *Introduction to Laboratory Cryogenics.* Janis Research Company, 1990.

[23] R. Sherwin, R. J. H. Clark, R. Lauck, and M. Cardona. Effect of Isotope Substitution and Doping on the Raman Spectrum of Galena (PbS). To be published.

[24] R. B. Schoolar and J. R. Dixon. Optical Constants of Lead Sulfide in the Fundamental Absorption Edge Region. *Phys. Rev.*, 137:A667, 1965.

[25] J. Serrano, C. Schweitzer, C. T. Lin, K. Reimann, M. Cardona, and D. Fröhlich. Electron-Phonon Renormalization of the Absorption Edge of the Cuprous Halides. *Phys. Rev. B*, 65:125110, 2002.

[26] G. I. Peresada, E. G. Ponyatovskii, and Z. D. Sokolovskaya. Pressure Dependence of the Eleastic Constants of PbS. *Phys. Stat. Sol. (a)*, 35:K177, 1976.

[27] V. Prakash. Technical Report No HP-13 from the Division of Engineering and Applied Physics. Havard University, 1967.

[28] D. L. Mitchell, E. D. Palik, and J. N. Zemel. Magneto-Optical Band Studies of Epitaxial PbS, PbSe and PbTe. *Proc. 7th Int. Conf. Phys. Semicond*, 325, 1964.

[29] S. I. Novikova and N. K. Abrikosov. Investigation of the Thermal Expansion in Lead Chalcogenides. *Sov. Phys. Solid State*, 5:1397, 1964.

[30] M. M. Elcombe. The Crystal Dynamics of Lead Sulphide. *Proc. Royal. Soc. London A*, 300:210, 1967.

[31] K. S. Upadhyaya, M. Yadav, and G. K. Upadhyaya. Lattice Dynamics of IV-VI Ionic Semiconductors: An Application to Lead Chalcogenides. *Phys. Stat. Sol. (b)*, 229:1129, 2002.